Chapter 8

Aging and Degradation Behavior Elucidated by Viscoelasticity Aiming Protection of Smart City Facilities

Yukitoshi Takeshita, Takashi Miwa, Azusa Ishii and Takashi Sawada

Additional information is available at the end of the chapter

http://dx.doi.org/10.5772/65214

Abstract

Polymer coatings play a crucially important role in protecting smart city facilities against the harsh factors of outdoor environments. Recent increased awareness of eco-friendliness has led to the use of waterborne organic coatings. Research into the bulk material properties of these coatings is necessary in order to understand their degradation process in the field. The present work focuses attention on a unique rheological property, which has both elastic and viscous characteristics, as a means of assessing the stability of the coating. The viscoelastic property determines whether it presents solid-like or liquid-like response from the comparison of relative strengths of the relaxation time (τ) and operating time (t). In the process of degradation, both the storage (E′) and loss modulus (E″), which represent the elastic and viscous components, respectively, decrease accordingly, reflecting the deterioration of coating. The majority of the water molecules absorbed in a coating are strongly bound to the polymer network through hydrogen bonds with polar functional groups, which destroys intermolecular bonding between macromolecules and reduces the bulk materials' ability to diffuse stress concentrations and thereby lowers a coating's overall strength.

Keywords: rheology, static and dynamic viscoelasticity, aging and degradation, water diffusion and absorption, FT-IR, DSC

1. Introduction

In providing telecommunications services throughout Japan, NTT utilizes enormous numbers of telecommunications plants and materials, including approximately two-million kilometers of cable and nearly 12 million telephone poles [1]. Outdoor materials in particular are exposed

to a wide range of environments: UV light, a range of temperatures and humidity, sea salt particles, alkalinity, and acidity. Therefore, these materials are protected by some type of weathering-prevention technology, and a wide variety of anti-corrosion technologies have been developed for each type of environment [2].

Polymeric materials are available for coating onto large steel structures, such as road and railway bridges, and electric power and telephone poles, which form a part of the social infrastructure in smart cities. We have therefore developed and introduced organic coatings for use in industrial telecommunications facilities [3–7].

The coatings typically have a multilayer structure, with the bottom layers functioning to bond the coating to the steel substrate and the top layers providing primary protection and pigmentation. Conventional coatings usually include a wide variety of volatile organic compounds (VOC), such as hydrocarbons (hexane, toluene, xylene), ketones (acetone, methyl ethyl ketone, methyl isobutyl ketone), alcohols (methanol, ethanol, cyclohexanol), and esters (ethyl acetate, butyl acetate, isobutyl acetate) [8]. VOCs are environmentally damaging and pose human health risks. So, an awareness of the importance of being eco-friendly has been growing even in the coating fields.

One solution is to reduce the proportion of solvent in the coating, ultimately to zero, and we have already developed and introduced a low-solvent coating for use in the telecommunications field. Another solution is to replace organic solvents with water. Water-based coatings have been in high demand, and we have therefore been studying them with a view to protecting human health and the environment [3–7, 9–11]. Research into the bulk material properties of these low-VOC coatings is necessary to understand their degradation process.

In engineering applications of polymeric materials, physical aging commonly arises throughout the service lifetime of the component. Physical aging is proposed to be a long-term relaxation process that occurs in polymers in a glassy state below the glass transition temperature (T_g) as the macromolecules gradually approach thermodynamic equilibrium [12]. This aging is the main phenomenon affecting the physical stability of polymeric materials and thus of organic coatings, and it is accepted that this phenomenon has an impact on the formulation, application, and service life of organic coatings. While the studies reported to date clearly indicate the considerable practical importance of the aging phenomenon in relation to degradation behavior and failure, theoretical and practical questions remain unsolved [12, 13].

The present work focuses on the effect of aging and further degradation on the rheological property of mainly epoxy/urethane coating film, which is targeted for use in telecommunications fields. The static and dynamic viscoelastic properties are intensively evaluated in an accelerated weathering condition, and the correlation between degradation behaviors and rheological properties is discussed. Finally, the states of water absorbed in coating as an aggressive factor affecting property of coating are represented using differential scanning calorimetry (DSC) and Fourier transform infrared (FTIR) spectroscopy.

http://dx.doi.org/10.5772/65214

2. Past research

Physical aging is an important factor in relation to the physical properties of many polymers at room temperature, which is below T_g [14–17]. A lot of past researches have investigated the physical aging of polymers including polyethylene [18, 19], epoxy [20–22], poly(methyl methacrylate) [23, 24], polyester [25, 26], poly(vinyl acetate) [27], powder coatings [28, 29], and organic coatings [12, 30–35]. There has been a great deal of excellent work on the spontaneous relaxation process of coating films during physical aging [12, 14, 18–20, 28–31]. Skaja has published outstanding basic work designed to determine the relationship between changes in bulk mechanical properties and degradation during the accelerated weathering of coating films [31].

In research on adhesives, it has been well established through many studies that the performance of pressure-sensitive adhesives (e.g., peel, tack, and shear) depends strongly on the bulk viscoelastic properties of the adhesives [36–45]. Further, as regards wood research, Mizumachi et al. have suggested that adhesive strength is strongly dependent on the rheological properties of the adhesives [46–54]. However, the exact relationship between rheological performance and degradation behavior for eco-friendly coating film has not been established.

3. Theory

3.1. Physical aging

The basic thermodynamic description of the state of the glass for polymers has been universally accepted for many years. Indeed, the earliest thermodynamic treatments by Davies and Jones [55, 56] remain among the best available. Perera has reported theoretical considerations on physical aging of polymer [12].

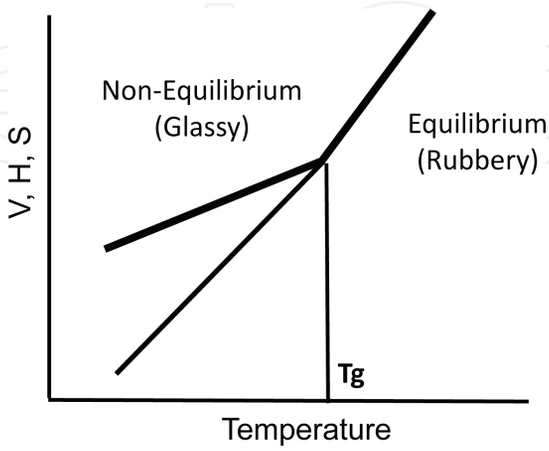

Figure 1. Schematic representation of the dependence of volume (V), enthalpy (H) and entropy (S) on temperature, based on Perera [12].

Polymer volume (V), enthalpy (H), and entropy (S) are represented as a function of temperature (T) as shown in **Figure 1**. During cooling, V, H, and S behave differently at temperatures above and below T_g. At $T>T_g$, the decrease in V, H, and S can follow the decrease in temperature due to higher mobility of macromolecular chains, and thus the polymer is in equilibrium state. At $T<T_g$, due to lower mobility of macromolecular chains, the decrease in V, H, and S cannot follow the decrease in temperature and thus the polymer is in a nonequilibrium state. In this state, molecular motion is limited but does not stop and continues toward an equilibrium state. This spontaneous process has been known under many terms, such as volume relaxation, enthalpy relaxation, mechanical relaxation, and structural relaxation. These relaxations are referred as "physical aging" [12].

3.2. Rheology

Rheology is the study addressing the deformation and the flow of materials [57]. It applies to substances with a complex microstructure, such as muds, sludges, suspensions, polymers, and other glass formers, as well as to many foods and additives, bodily fluids, and other biological materials, or to other materials in the class of soft matter. The rheological response is expressed as the combination of elastic and viscous components which has elastic modulus and viscosity. It is normally represented using Maxwell model consisting of a spring with modulus E in series with a dashpot with viscosity η [**Figure 2(a)**] and Voigt model consisting of a spring in parallel with a dashpot [**Figure 2(b)**].

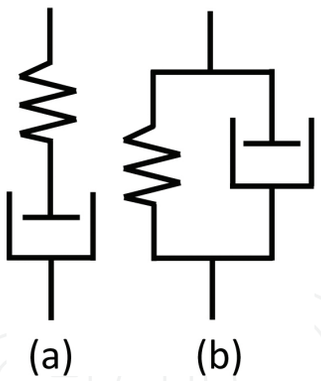

Figure 2. Diagram of viscoelastic material. (a) Maxwell model and (b) Voigt model.

3.2.1. Static viscoelasticity

3.2.1.1. Maxwell model

When constant strain ε is applied to Maxwell model, stress σ in each component is expressed as:

$$\sigma = E\,\varepsilon_1 \tag{1}$$

http://dx.doi.org/10.5772/65214

$$\sigma = \eta \frac{d\varepsilon_2}{dt} \tag{2}$$

where

$$\varepsilon = \varepsilon_1 + \varepsilon_2 \tag{3}$$

E and η are elastic modulus and viscosity. By solving simultaneous Eqs. (1)–(3),

$$\sigma = \sigma_0 e^{-t/\tau} \tag{4}$$

where σ_0 is an initial stress, t is time, and τ is relaxation time, η/E.

3.2.1.2. Voigt model

When constant stress σ is applied to Voigt model, stress in each component is expressed as:

$$\sigma_1 = E\,\varepsilon \tag{5}$$

$$\sigma_2 = \eta \frac{d\varepsilon}{dt} \tag{6}$$

where

$$\sigma = \sigma_1 + \sigma_2 \tag{7}$$

By solving simultaneous Eqs (5)–(7),

$$\varepsilon = \frac{\sigma_0}{E}\left\{1 - e^{-t/\tau}\right\} \tag{8}$$

3.2.2. Dynamic viscoelasticity

When sinusoidal strain ε expressed as:

$$\varepsilon = \varepsilon_0 e^{i\omega t} \tag{9}$$

is given to Maxwell model,

$$\sigma = \sigma_0 e^{i(\omega t+\delta)} \tag{10}$$

where $i = \sqrt{-1}$, ω and δ are the angular velocity and phase difference. By solving simultaneous Eqs (1)–(3), (9) and (10), complex modulus E* is expressed as:

$$E^* = \sigma / \varepsilon = \left(\frac{\omega^2\tau^2}{1+\omega^2\tau^2} + i\frac{\omega\tau}{1+\omega^2\tau^2} \right) E = E' + iE'' \tag{11}$$

where E′ is the storage modulus $\left(= \frac{\omega^2\tau^2}{1+\omega^2\tau^2}E \right)$ and E″ is the loss modulus $\left(= \frac{\omega\tau}{1+\omega^2\tau^2}E \right)$.

Figure 3 shows E′/E and E″/E vs ωτ. At low frequency, the model behaves more viscously, while at high frequency, it behaves more elastically. In this work, stress σ in Eq. (4), storage modulus E′ and loss modulus E″ in Eq. (11), and loss tangent tanδ (E″/E′) are essentially discussed.

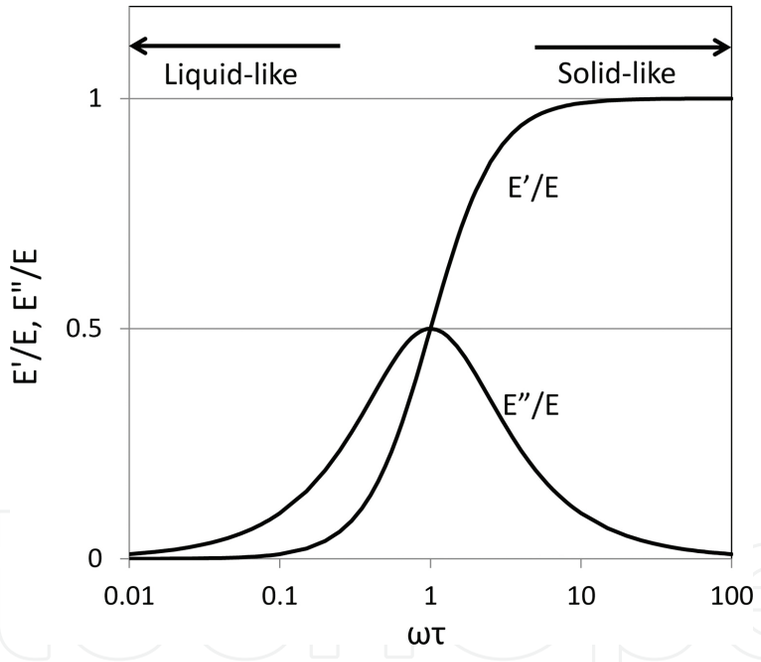

Figure 3. E′/E, E″/E vs. ωτ for Maxwell model.

4. Dynamic viscoelasticity in physical aging

To understand the basics of the behaviors of coating aged at room temperature, the dynamic viscoelastic properties, E′ and tanδ, were determined using a Rheolograph Solid (S-1, Toyo-seiki, Tokyo, Japan) [5]. The initial tension and dynamic strain are 60 gf (0.588N) and 8 μm, respectively. Coating films A, B, and C are all eco-friendly waterborne coatings. Each comprises

http://dx.doi.org/10.5772/65214

a bottom, middle, and top layer. The structures are respectively epoxy/epoxy/inorganic with total thickness of 130 μm for A, epoxy/epoxy/urethane with 125 μm for B, and acryl/acryl-styrene/acryl-urethane with 275 μm for C. **Figure 4(a)** and **(b)** shows the effect of aging on E′ and tanδ for coating film from 3 to 48 days old. Only the results for 100 Hz are shown for a discussion of the overall trend, though measurements for four frequencies, 100, 10, 1, and 0.1 Hz, were performed.

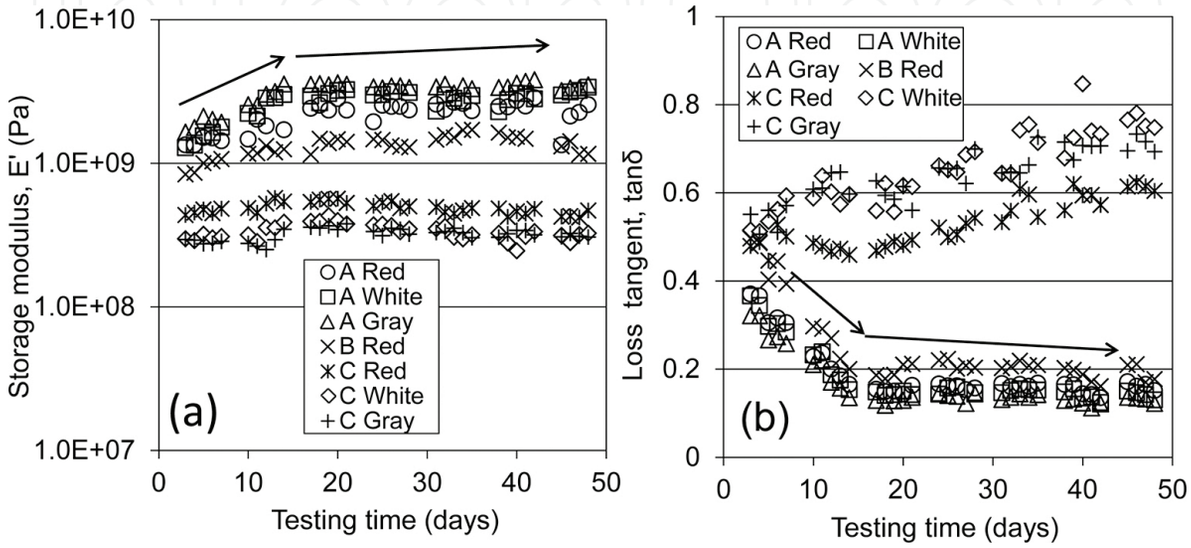

Figure 4. Effect of aging on E′ and tanδ for coating film aged 3–48 days at 100 Hz. (a) E′ and (b) tan δ [5].

From **Figure 4(a)**, it can be seen that the viscoelastic properties of A and B change rapidly for the first few days after preparation and then stabilize after a few weeks. After this, the sample no longer changes much with age. Although the data are not presented here, lower frequencies experience greater changes with increasing sample age, though stability occurs at the same age. **Figure 4(b)** shows that tanδ for A and B decreases with age, though it does so at low frequencies equally.

It is considered that the viscoelastic properties of A and B change because of the evaporation of the solvent that remained in the coating matrix. As the solvent evaporates, the film becomes hard and rigid and exhibits a high E′. In addition, the densification and the cross-link reaction might proceed [12]. As a result, the elastic property increased, corresponding to the increase in E′, and the viscous property decreased, corresponding to the decrease in tanδ. Once the solvent has completely evaporated, it might no longer affect the viscoelastic properties and become stable.

Film C exhibits very different trends. From **Figure 4(a)**, its E′ value seems to change very little with age. In addition, tanδ increases with age as shown in **Figure 4(b)**. We believe that C fundamentally has a strong viscous feature compared with A and B. Therefore, even after considerable time has elapsed, it is only slightly more rigid than at the beginning. As described in the previous section, E′ generally represents the elastic feature and E″, thus tanδ, indicates

the viscous one. At a simple level, it can determine the characteristics representing the nature of a film which has solidity or softness from dynamic viscoelastic measurements.

As coatings A and B exhibit the elastic property, the relaxation time τ is considered here. From **Figure 3**, the region that represents the elastic property is the right area where x values are around 5–100:

$$5 < \omega\tau < 100 \tag{12}$$

The frequency f applied here is 100 Hz, so angular velocity ω is obtained by the following equation.

$$\omega = 2\pi f \fallingdotseq 628 \tag{13}$$

From Eqs. (12) and (13), the relaxation time τ is expressed as follows:

$$0.008\ (\fallingdotseq 0.01) < \tau < 0.16 \tag{14}$$

Operating time t is the reciprocal of the frequency, which is 0.01(=1/100) (s). Therefore, the following relation is introduced.

$$\left[Relaxation\ time\ (\tau)\right] > \left[Operating\ time\ (t)\right]$$

From this relation that relaxation time is higher than operating time, it is understood that the material does not flow (not relax) and thus presents a solid-like response and behaves as an elastic body.

Similarly, for coating C, the region that represents the viscous property is the left area where x values are around 0.01–0.5:

$$0.01 < \omega\tau < 0.5 \tag{15}$$

From Eqs. (13) and (15),

$$0.000016 < \tau < 0.0008 \tag{16}$$

As operating time t is 0.01 (=1/100) (s), the following relation is introduced.

$$\left[Relaxation\ time\ (\tau)\right] < \left[Operating\ time\ (t)\right]$$

http://dx.doi.org/10.5772/65214

That is, relaxation time is lower than operating time. This causes the material to flow (relax) and thus present a liquid-like response and behave as a viscous body.

Figure 5 illustrates the viscoelastic properties with the failure modes. At high E′, the breaking location is the bulk region of the layer. For high tanδ, it is the interface of the two layers. It is considered that E′ corresponds to the rigidity of the bulk material and the inability to release another material at an interface; tanδ is related to both the ability of the material to adjust to suit stress and to grasp another layer at the interface. Therefore, a high E′ indicates a high likelihood of failure within bulk planes, and a high tanδ increases the likelihood of failure within interface planes. A high contrast between the E′ values of sequential layers (high E′ and low E′) also increases the interface failure rate.

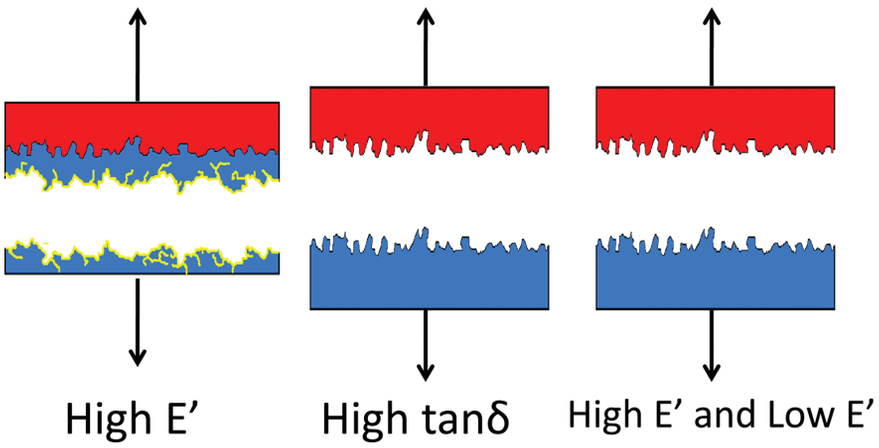

Figure 5. Viscoelastic properties and failure mode.

5. Behavior in heat cycling test

Figure 6 shows viscoelastic values of E′ and E″ of waterborne epoxy/acryl-urethane with 100-μm thickness under a heat cycling test that repeats a cycle from -30 to 70°C [6], where one cycle takes 12 h. Relative humidity reaches 90% at high temperature of 70°C and is almost 0% below 0°C. **Figure 6** shows that E′ increases at 50 cycles and then decreases at 100 cycles. In particular, several small cracks are observed on the coating at 100 cycles. In addition, T_g increases at around 50°C at 50 cycles; however, it does not vary from 50 to 100 cycles. Taking the results in **Figure 4** into account, the region of 0–50 cycles exhibits an increase in E′ and decrease in E″, similar to the aging behavior observed in coatings A and B in **Figure 4**; however, the region of 50–100 cycles shows dissimilar degradation behavior, where both E′ and E″ decrease due to water absorption.

It is found that the heat cycling accelerates degradation more than room-temperature aging does. To determine the effect of dry and wet states under the heat cycling condition, the degradation behavior under constant humidity, dry or wet, was investigated [7]. Two tests were performed: one was a dry heat cycle where humidity was 10% constant and the temper-

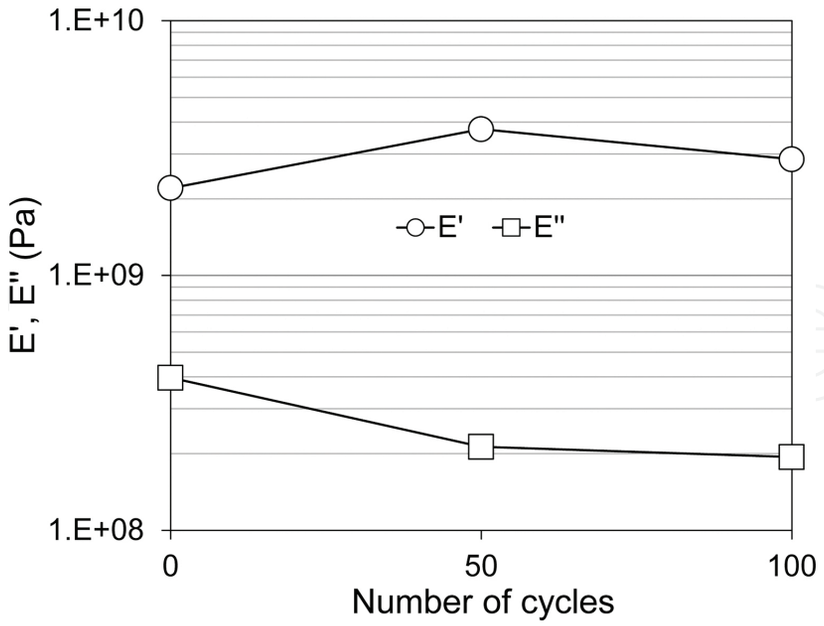

Figure 6. Effect of heat cycling test on E′ and E″ for epoxy/acryl-urethane [6].

ature was repeated from 10 to 70°C (Test 1), and the other was a wet heat cycle where humidity was 95% constant and the temperature was repeated from 10 to 70°C in the same way (Test 2). E′ and tanδ values are shown in **Figure 7**. The coatings are all epoxy/epoxy/urethane. A and B are waterborne coatings where the epoxy equivalent ratio is smaller for A than for B. C and D are strong and weak solvent types, respectively. **Figure 7** shows that E′ once increases and then stabilizes with age, similar to its behavior in **Figure 4**. Accordingly, tanδ rapidly decreases and then stabilizes. These behaviors are similar to those in coatings A and B in **Figure 4** and in the first half period (0–50 cycles) in **Figure 6**. Strict comparison elucidates that the degrees of increase in E′ and decrease in tanδ are larger in the wet state than in the dry one. Therefore, a comparison of T_g values is shown in **Figure 8**. The peak temperature indicates T_g. Tests 1 and 2 were dry and wet states, respectively. The increase in T_g is obviously larger in the wet state than in the dry one [(a) wet 30°C > dry 20°C; (b) wet 35°C > dry 30°C; (c) wet 45°C > dry 25°C; (d) wet 15°C > dry 10°C]. Thus, the increase in E′ is attributed to curing and hardening of the coating, which causes high T_g that are facilitated remarkably in the wet state more than in the dry state. Densification also accounts for the high T_g. This densification needs high mobility of macromolecule segments. It is also considered that the wet state helps macromolecule movement.

To determine experimentally whether densification proceeds, DSC was performed. **Figure 9** shows the thermal analysis in DSC. Densification can be detected by enthalpy relaxation that shows an endothermic peak due to absorbing the heat in the sub-T_g region. Black arrows certainly indicate the enthalpy relaxation in waterborne coatings A and B in **Figure 9**. However, solvent-type coatings C and D do not exhibit it. Instead, an endothermic peak due to evaporation of the solvent is observed as indicated by the white arrow. Therefore, for waterborne coating, high T_g is partly due to densification, whereas, for solvent-type coating, it is somewhat due to solvent evaporation.

http://dx.doi.org/10.5772/65214

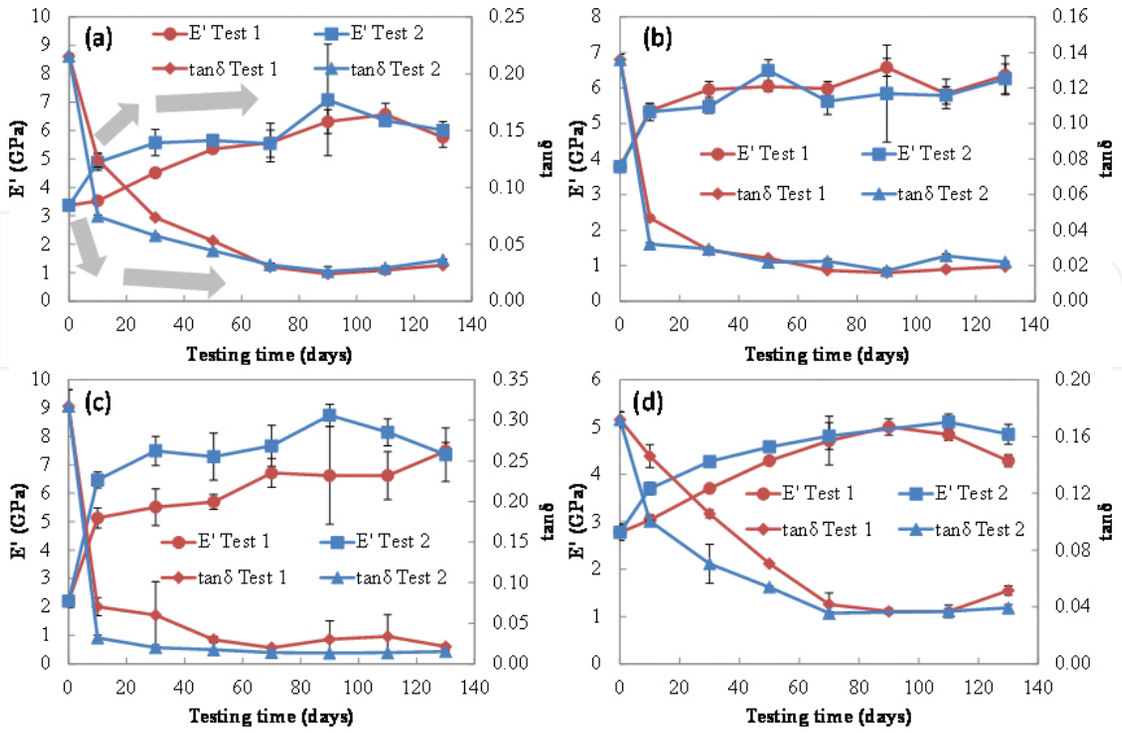

Figure 7. E′ and tan δ in heat cycling test. Test 1: dry. Test 2: wet. (a) Coating A, (b) coating B, (c) coating C, (d) coating D [7].

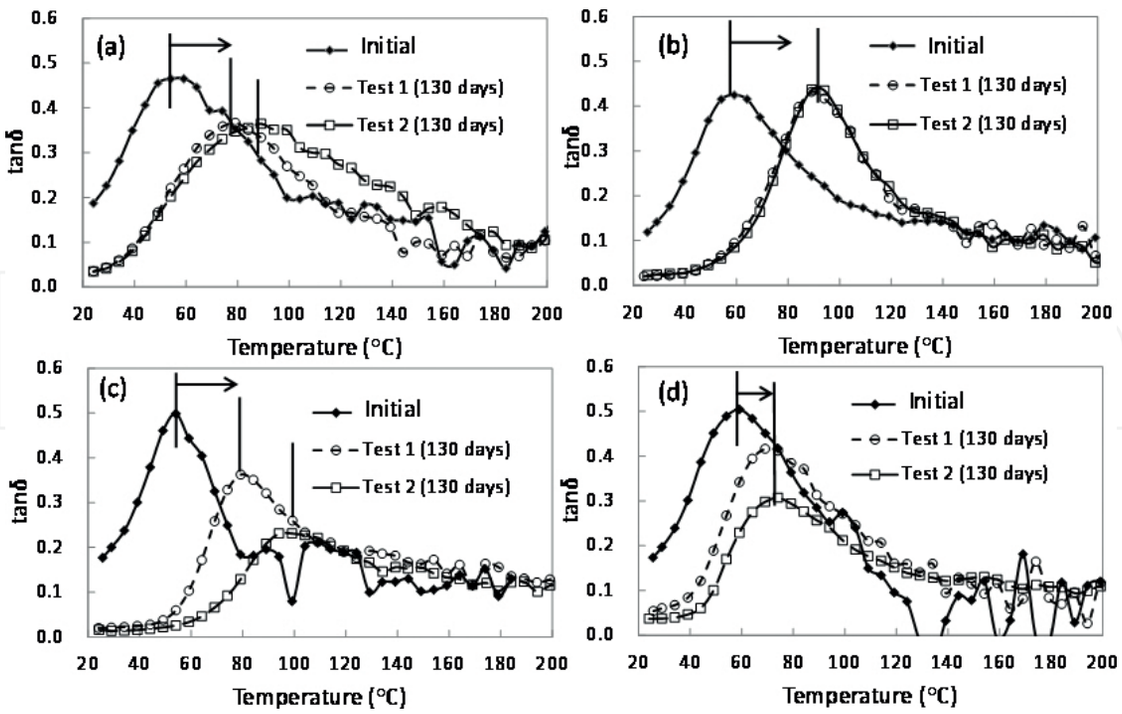

Figure 8. Temperature dependence of tan δ at 130 days in heat cycling test. Test 1: dry. Test 2: wet. (a) Coating A, (b) coating B, (c) coating C, (d) coating D [7].

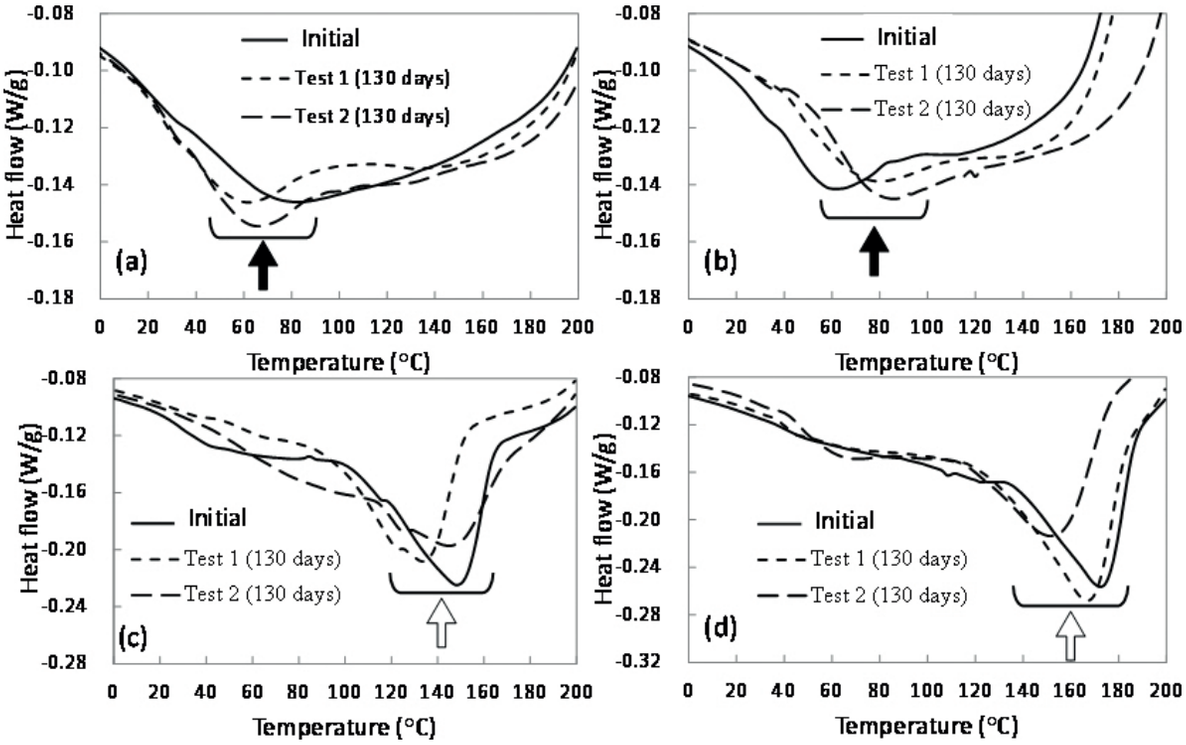

Figure 9. DSC curves at 130 days in heat cycling test. Test 1: dry. Test 2: wet. (a) Coating A, (b) coating B, (c) coating C, (d) coating D [7].

6. Effect of water molecules

As it is understood that the high-moisture state accelerates the aging and degradation behaviors, the influence of water molecules is focused on in this section [9]. The water diffusion process and saturated water content, as well as adhesive strength, are investigated.

Figure 10 shows the nature of water diffusing in coating film. Coatings A and B are epoxy/epoxy/urethane with 125-μm thickness and epoxy/epoxy/fluororesin with 140-μm thickness, respectively. Both are waterborne coatings. From **Figure 10**, water content M_t increases with time and stabilizes around 50–100 h. The saturated contents M_∞ of A and B are 6.6% and 3.7%, respectively. The higher M_∞ of coating A is attributed to higher water absorption of urethane than that of the fluororesin of the top layer. Bottom layers are both epoxy, but the polarity of the epoxy of A is likely higher than that of B. **Figure 11** shows the aging time dependence of M_∞. The longer the time is, the lower the M_∞ value becomes (100 days: A 8.5%, B 5.5% > 200 days: A 6.6%, B 3.7%). The decrease in M_∞ is caused by the densification of macromolecules. This densification process progresses over aging time due to the relaxation of macromolecule segments that occurs in the coatings glassy state [12]. As the densification progresses, the β transition peak shifts to a higher temperature, which is a phenomenon that has been observed in our research. This agrees with the above aging time dependence of M_∞ in **Figure 11**.

http://dx.doi.org/10.5772/65214

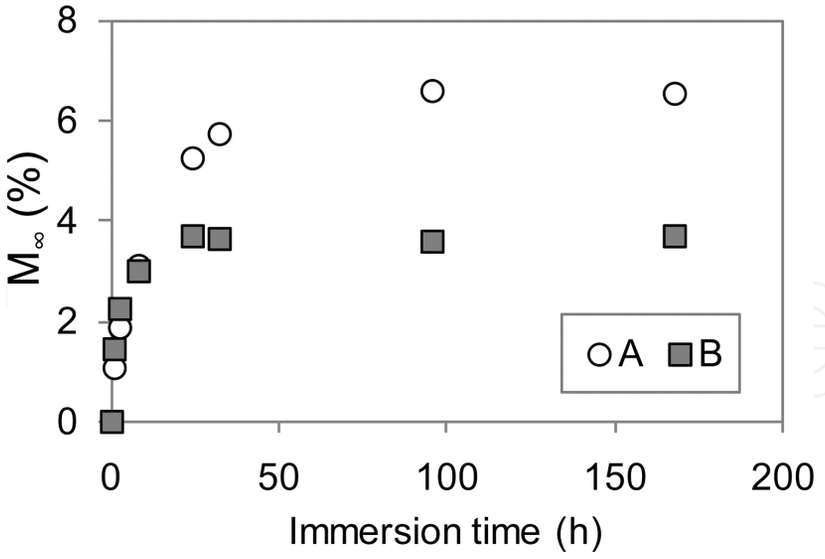

Figure 10. Water absorption behavior. A epoxy/epoxy/urethane. B epoxy/epoxy/fluororesin [9].

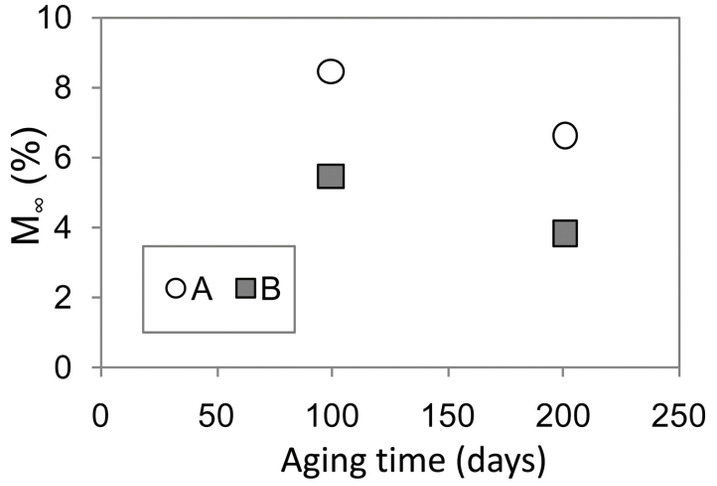

Figure 11. Aging time dependence of saturated water content. A epoxy/epoxy/urethane. B epoxy/epoxy/fluororesin [9].

The dynamics of water diffusion is studied next. The M_t/M_∞ linearly increases at the early stage of absorption and steadily approaches equilibrium. This feature indicates that water absorption exhibits Fickian diffusion [58] and the diffusion coefficient D can be calculated from the slope of plot of M_t/M_∞ vs $t^{1/2}l^{-1}$, where l is film thickness. D values of A and B are 7.39×10^{-14} and 24.2×10^{-14} m^2/s, that is, A < B, which is opposite to the saturated water content, M_∞. The difference in D seems to be due to the difference in the cross-link density. By measurement of E′ in the plateau region of E′ vs temperature, it is found that the cross-link densities are around 5300 and 2600 mol/m^3 for A and B. That is, the lower D shows the higher crosslink density. This result suggests that higher crosslink density prevents water molecules from easily diffusing.

In relation to the mechanical properties in water absorption, **Figure 12** shows adhesive strengths, which agree with the trends in the E′ values. Adhesive strengths once increase at 50

cycles and then decrease at 100 cycles. At 100 cycles, they are 0.8 and 3.7 MPa for A and B, which is A < B. Taking the results of A > B for M_∞ and A < B for *D* into account, it is clear that the M_∞ value affects the degraded adhesive performance much more than the *D* value does. This might be because the water content is saturated for most of the moisture period in the test.

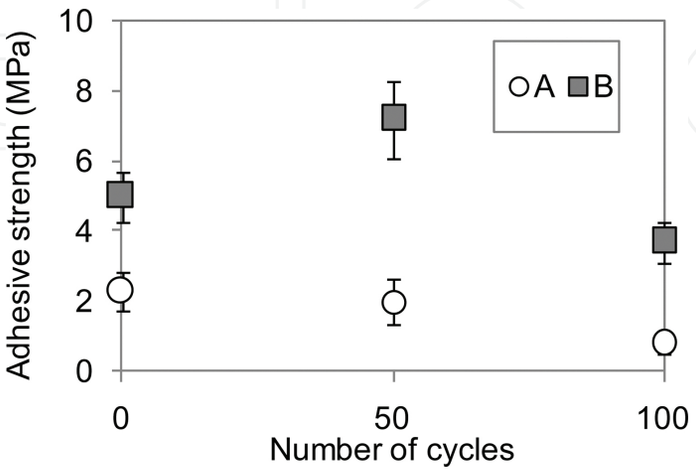

Figure 12. Adhesive strength in heat cycling test. A epoxy/epoxy/urethane. B epoxy/epoxy/fluororesin [9].

7. Static viscoelasticity during water absorption

As it is understood that the saturated water significantly affects the deterioration of E′ and adhesive strength, we focus attention on water molecules as an aggressive factor in this section [10]. That is, we attempt to determine their contribution to static stress relaxation behavior as a mechanical property of coatings.

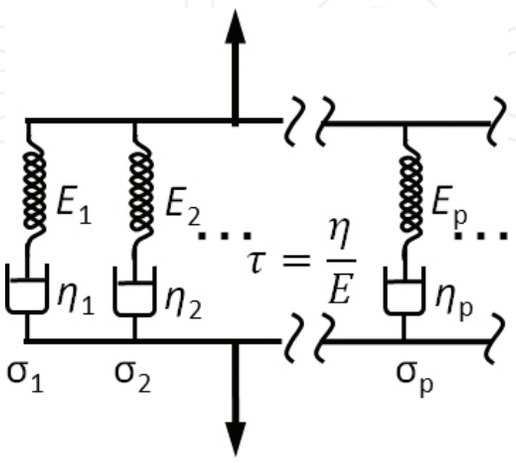

Figure 13. Diagram of generalized Maxwell model for viscoelastic material.

http://dx.doi.org/10.5772/65214

Stress relaxation behavior can be described by a simple Maxwell model of viscoelastic material using an exponential decay function [59]. The stress will decay exponentially, with a relaxation time τ, as described by Eq. (4). Expansion to a generalized Maxwell model, or Maxwell-Weichert model, which consists of several Maxwell model components with different E and η values in parallel, as shown in **Figure 13**, produces a function where the relaxation behavior is described as a superposition of multiple exponentially decaying modes:

$$\sigma(t)/\sigma_0 = \sum_{p=1}^{p\geq 1} g_p \; e^{-\left(t/\tau_p\right)} \tag{17}$$

where τ_p is the relaxation time and g_p is the normalized intensity of the p^{th} relaxation mode. The complex nature of the equation typically results in its being simplified into a stretched exponential function, commonly called the William-Watts (W-W) equation [60]:

$$\varphi(t) = \sigma(t)/\sigma_0 = e^{-(t/\tau)^{\beta}} \tag{18}$$

Here, stretching exponent β, with bounds 0< β<1, represents the relative distribution of the relaxation modes; a decrease in β corresponds to an increase in the distribution of relaxation times, τ_p, of the individual components of the system [61–64]. In this equation, τ represents a "characteristic relaxation time" for the system as a whole. The φ(t) is the ratio of the stress at a time "t" to the initial stress.

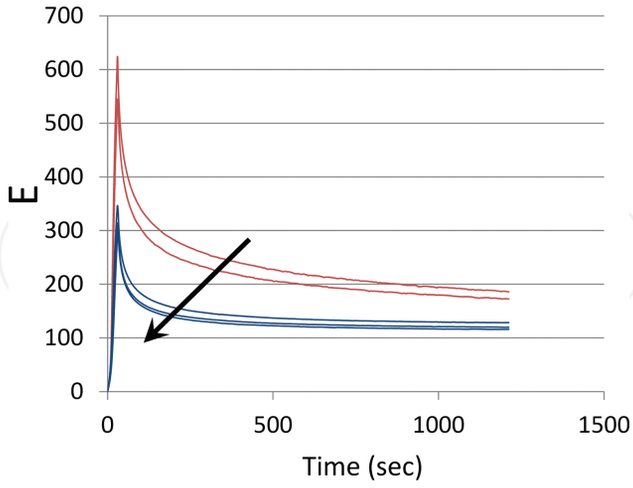

Figure 14. Stress relaxation curves [10].

The three parameters of this equation—σ_0, τ, and β,—are not independent; thus, it is necessary to determine one parameter independently before solving for the other two [15]. In this experiment, σ_0 was taken to be the maximum stress attained by the sample during testing. It

may actually be higher as some relaxation occurs as the sample is being drawn; however, this approximation is close enough to provide an accurate description of the behavior of the sample. We measured the changes in the three parameters during water absorption and considered their contribution to the degradation behavior.

The four coatings—A, B, C, and D—are the same as those in section 5. Stress relaxation curves are shown in **Figure 14**. E(t) exponentially decreases with time, which is quite reasonable. With water absorption, the curves shift as indicated by the arrow. The three parameters of the stretched exponential function, E_o, τ, and β, are determined to fit the stress relaxation behavior and plotted as a function of M_t/M_∞ in **Figure 15**. E_o and β quickly decrease in the early stages between $M_t/M_\infty = 0$ and $M_t/M_\infty \approx 0.5$ and level off later between $M_t/M_\infty \approx 0.5$ and $M_t/M_\infty \approx 1$, as shown in **Figure 15(a)** and **(c)**, while τ exhibits a roughly exponential increase between $M_t/M_\infty = 0$ and $M_t/M_\infty \approx 1$, as shown in **Figure 15(b)**.

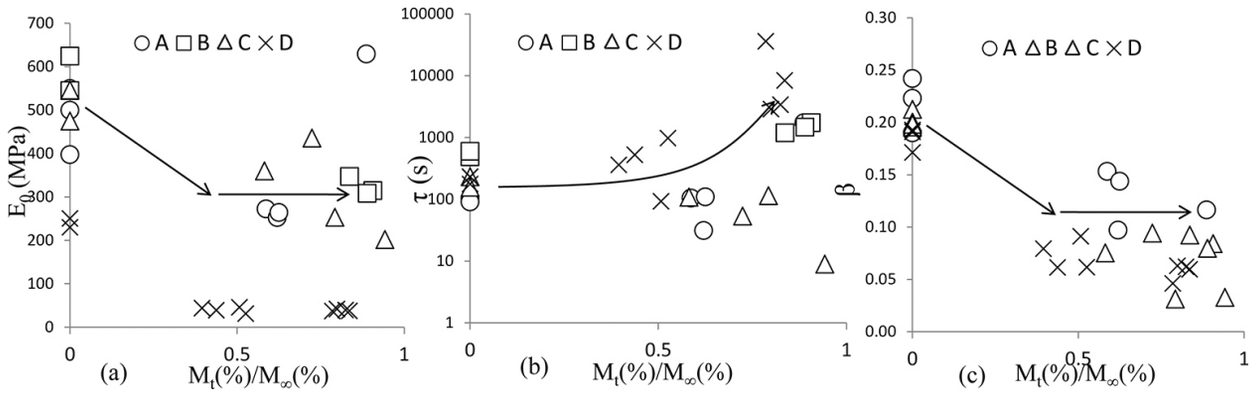

Figure 15. E_o, τ, and β as a function of water content. (a) E_o, (b) τ, (c) β [10].

Water is commonly considered to act as a plasticizing agent in polymers [65–69], which caused a decrease in E_0 in all the samples as M_t/M_∞ approached 1, which is quite reasonable.

Molecular interactions between polymer chains, such as hydrogen and dipole-dipole bonding, cause some degree of reduction in chain mobility [70]. This has the effect of "averaging" or decreasing the distribution of the relaxation times for the individual components of the system. The introduction of water into the polymer network interrupts the intermolecular bonding [66, 71, 72], which reduces this averaging effect and results in the reduction in β for the system as a whole. Water that is bonded to polymer chains interrupts molecular interactions between polymer chains, which contributes to changes in the bulk material properties. Free water, on the other hand, has little effect on polymer chains and little influence on the material properties [71, 73]. The details of behaviors of free water as well as bonded water molecules are described in the next section. As for increase in relaxation time τ in **Figure 15(b)**, absorbed water causes the decrease in restoring force of the elastic component in Maxwell model, which hinders a smooth recovery of the spring component.

The adhesive strength of dry and saturated samples is shown in **Figure 16**. The adhesive strength decreases with water absorption. This indicates that absorbed water has a highly

http://dx.doi.org/10.5772/65214

detrimental effect on adhesive strength. As previously asserted, absorbed water interferes with the intermolecular interactions of the polymer. Cross-linking, in addition to narrowing the distribution of relaxation times, may also narrow the distribution of elastic moduli to assist the diffusion of stress concentrations. As described in Eq. (17), each polymer chain, or mode of the system, has its own elastic modulus, which likely follows a distribution similar to the distribution of τ.

Stress applied to the system will concentrate the largest force in the mode with the highest elastic modulus. Molecular interactions between polymer chains in the system likely help to diffuse this stress concentration. In a saturated system, where the interactions are interrupted, an increase in stress concentration would cause areas of high stress to fail, with the failure propagating through the polymer along a plane perpendicular to the applied stress.

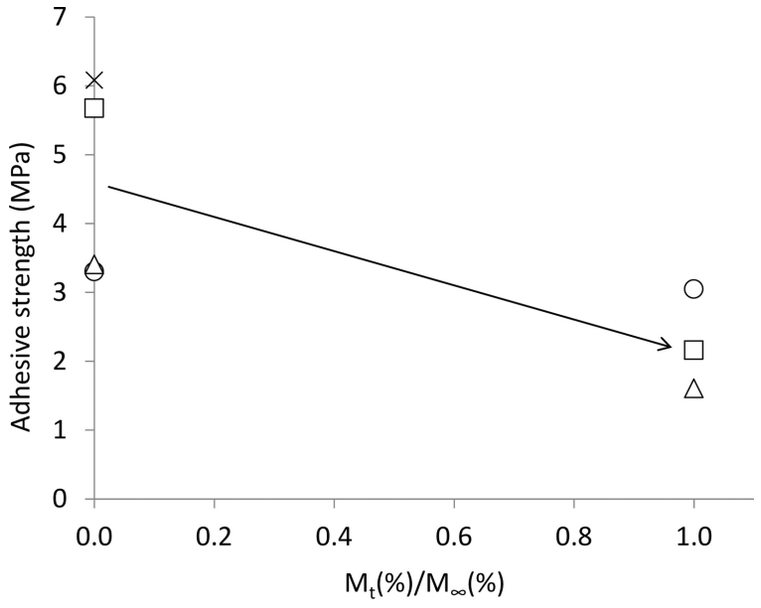

Figure 16. Adhesive strength vs. water content [10].

8. States of water absorbed in coating

As it is understood that water molecules absorbed into the polymer network interrupt the intermolecular bonding, which causes degradation of mechanical properties, we attempt to estimate the manner in which absorbed water bonds to the polymer network [11]. That is, we characterize the absorbed water into states based on the results of DSC and attenuated total reflection (ATR) FT-IR spectroscopy.

Higuchi and Liu have reported that there are three ways the absorbed water exists within polymer [74–76]: one is as free water, which is free of any forces and whose freezing point is normally around 0°C; another is as weakly bound freezable water in which the water freezing point shifts to lower temperature due to intermolecular interaction between water molecules

and the polymer network. In our research, the temperature was between -40°C and -65°C, and the other is as strongly bound nonfreezable water, where the water molecules do not freeze at any temperature due to their strong bonds with the polymer network. The type and mass of each water molecule can be determined by observing the position and area of the exothermic peak in the DSC chart during the cooling process.

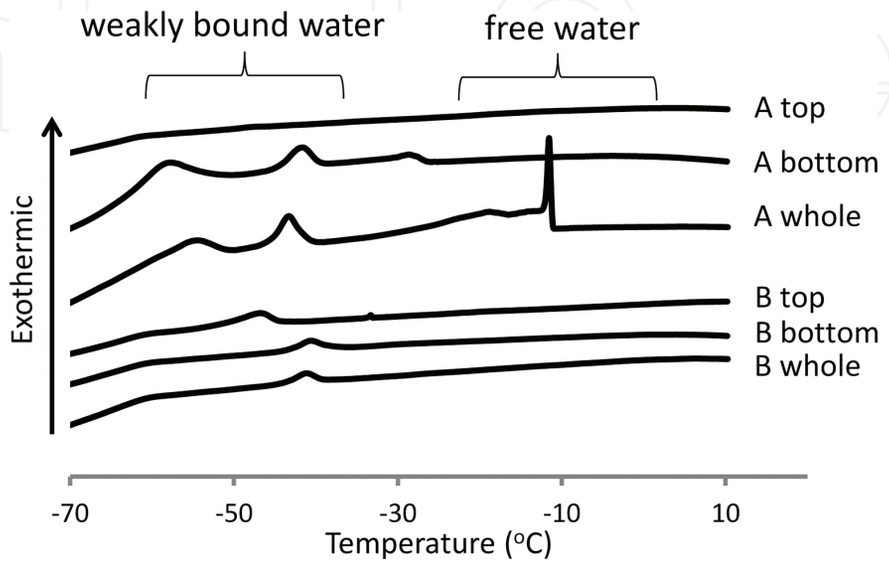

Figure 17. DSC curves for coating A and B during cooling process [11].

	Percentage (%)			
	Free	**Weak 1**	**Weak 2**	**Strong**
A top	0	0.3	0	99.7
A bottom	0	7.9	12.1	80.0
A whole	5.9	5.7	6.3	82.1
B top	0	8	0	92.0
B bottom	0	2.6	0	97.4
B whole	0	3.6	0	96.1

Table 1. Percentage of water in each state estimated by DSC when polymer is saturated with water [11].

Figure 17 shows the DSC curves for coatings A and B, which are the same as those in section 7. As seen in **Figure 17**, the free water is observed in A whole which is around −10°C. The peaks due to weakly bound freezable water are observed in A bottom, A whole, B top, B bottom, and B whole at around between −40°C and −65°C. Free water is not observed in coating B. **Table 1** shows numerically the percentage of water in each state estimated by DSC when polymer is saturated. Calculated values obtained from DSC measurements are compared with a gravimetric measurement of the total mass of absorbed water. The mass of water stored in each

http://dx.doi.org/10.5772/65214

observed DSC state is determined, and the remaining water is assumed to be stored in a strongly bound state. As seen in **Table 1**, most of the water molecules, above 80%, are strongly bound to the polymer network. The rest are weakly bound. Free water is present only between layers.

As for FT-IR analysis, Musto [77], Mijovic [78], and Cotugno [79] have reported that there are three types of water molecules, depending on the relative strength of intermolecular bonding to the polymer network, resulting in a difference in the wavelength of stretching vibration of O–H bonds of water molecules, S_0, S_1, and S_3. S_2 represents two hydrogen atoms participating in hydrogen bonding to polymer network. S_1 represents only one hydrogen atom participating in hydrogen bonding. S_0 represents that there are no hydrogen atoms participating in hydrogen bonding. S_2 can be detected at lower frequency due to strong hydrogen bonding, while S_0 can be at higher frequency due to weak hydrogen bonding. **Figure 18** shows a 2D correlation spectroscopy of FT-IR for the A top layer, which can determine the time-resolved correlation during water absorption between any two points of the spectrum. **Figure 18(a)** shows a synchronous correlation, which presents a correlation between changes in different peaks. **Figure 18(b)** shows an asynchronous correlation, which presents a phase difference between changes in different peaks. As seen in the synchronous plots in **Figure 18(a)**, absorbed water creates the largest peak at around 3460/cm^{-1}, which correlates to OH stretching vibration. There are two noticeable shoulders on the primary water peak, which indicates additional peaks centered at around 3260 and 3600/cm^{-1}. Based on the consideration mentioned above, these peaks correspond to S_1, S_2, and S_0 states at 3460, 3260, and 3600/cm^{-1}. In the asynchronous plots in **Figure 18(b)**, the S_2 shoulder shows a phase delay in its growth behind the S_1 peak. There is no significant asynchronous correlation between S_1 and S_0, which suggests that S_0 and S_1 form first and then S_2.

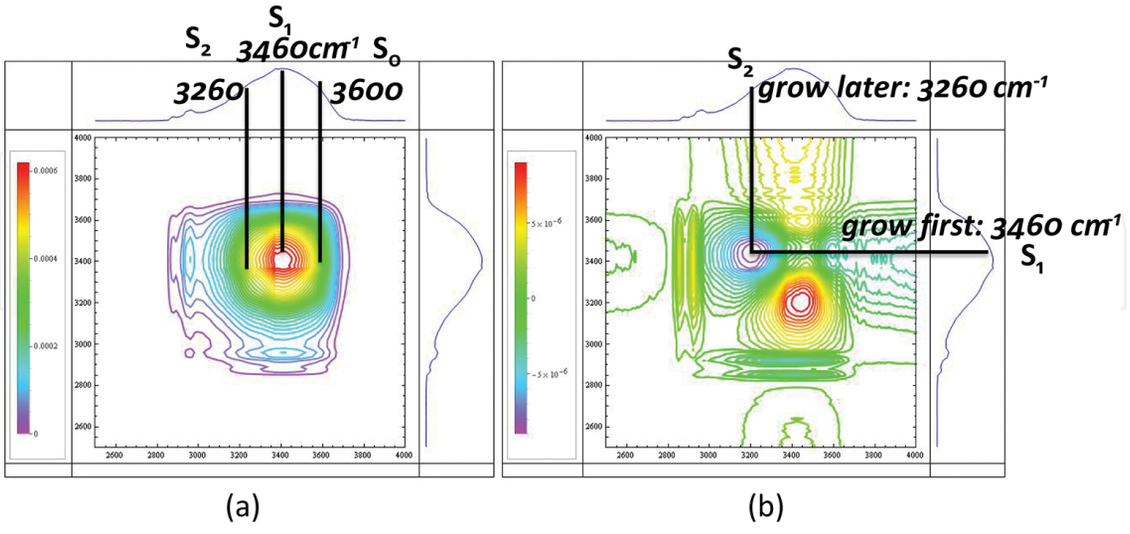

Figure 18. 2D correlation spectroscopy of FT-IR for A top layer. (a) Synchronous plot and (b) asynchronous plot [11].

From a comparison of areas of FT-IR peaks of S_0, S_1, and S_2 of A top, A bottom, B top, and B bottom, the relative strengths are $S_1 > S_2 > S_0$ for urethane and $S_2 > S_1 > S_0$ for epoxy. This indicates

that epoxy has more hydrophilic functional groups that present potential bonding sites for water molecule than urethane. Epoxy presents the groups for water, namely, tertiary and secondary amine, hydroxyl, and ether groups, while urethane presents the groups for water, namely, secondary amine, ether, and carbonyl groups.

Taken together, the DSC and FT-IR data indicate that six possible active functional groups are present in the epoxy/urethane coating system. Depending on the intensity, according to Harazaki [80], amine, hydroxyl, ether, carbonyl, and isocyanate groups provide sites for a strong DSC state due to hydrogen bonding. Epoxide groups provide sites for weak 2 due to dipole-dipole force. Other groups provide site for weak 1 due to van der Waals force. In addition, we speculate that all functional groups produce sites for the S_1 or S_2 state in FT-IR.

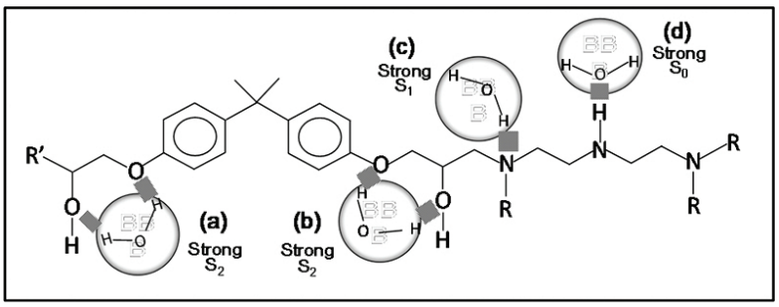

Figure 19. Image of water molecule absorbed in polymer network. (a) and (b) present strong DSC and S_2 FT-IR states, (c) presents strong DSC and S_1 FT IR states, and (d) presents strong DSC and S_0 FT IR states

Finally, an image of water molecules bonding to the polymer network is shown in **Figure 19**. In this image, water molecules (a) and (b) present strong DSC and S_2 FT-IR states, (c) presents strong DSC and S_1 FT-IR states, and (d) presents strong DSC and S_0 FT-IR states.

9. Conclusion

The rheological properties during aging of waterborne coatings at room temperature and during degradation in an artificially accelerated environment have been investigated, and the manner in which absorbed water bonds to the polymer network has been emphasized as an aggressive factor that causes degradation.

Viscoelastic properties represent that E′ and E″ vary intensively depending on the process of aging and degradation. During aging, E′ generally increases with time, while E″ decreases. In the process of degradation, both E′ and E″ decrease accordingly. The viscoelastic property determines whether it presents solid-like or liquid-like response from the comparison of relative strengths of the relaxation time (τ) and operating time (t). E′, E″, and tanδ can be used to evaluate likely planes of failure in multilayer combinations.

The majority of the water molecules are strongly bound to the polymer network through hydrogen bonds with polar functional groups, which destroys intermolecular bonding

between macromolecules and reduces the bulk materials ability to diffuse stress concentrations and thereby lowers a coating's overall strength.

Acknowledgements

The authors thank Dr. T. Handa and R. Nishio of NTT-AT and T. Kamisho of NTT East for their helpful discussions and Richard Jackson and Ethan Becker, interns from the University of Wisconsin Platteville, for their enthusiastic work in this research.

Author details

Yukitoshi Takeshita*, Takashi Miwa, Azusa Ishii and Takashi Sawada

*Address all correspondence to: takeshita.yukitoshi@lab.ntt.co.jp

NTT Device Innovation Center, NTT Corporation, Atsugi-shi, Kanagawa, Japan

References

[1] Takeshita Y, Xiaoxi Z, Sugiyama A, Sawada T: Increasing the lifetime and reliability of telecommunication plant materials. NTT Technical Review. 2010; Available from: https://www.ntt-review.jp/archive/ntttechnical.php?contents=ntr201301fa4_s.html [Accessed: 2015-05-01]

[2] NTT East Technical Support Center. 4 Material degradation. In: Trouble Q & A in Telecommunication Facilities. 2nd ed. The Telecommunication Association: Ohmsha; 2008. p. 309–415

[3] Takeshita Y, A study of rheological property for degradation of environmentally friendly coating. In :Proceedings of the Reports on Weathering Technology Achievements 2010; 25 November 2010; JWTC: Tokyo; 2010. p. 25–34

[4] Takeshita Y. Sakata S. Sawada T. Jackson Jr R. Nishio R. Rheological property and adhesive performance of polymer coating film for telecommunication plant. Corr. Eng. 2011; 60: 88–95. Allerton Press, Inc., 2011

[5] Takeshita Y. Jackson Jr R. Sakata S. Sawada T. Nishio R. Aging property of eco-friendly anticorrosion organic coating film for telecommunication plant. Polym. Eng. Sci. 2012; 52:572–580. doi: 10.1002/pen.22119

[6] Kamisho T. Takeshita Y. Sakata S. Sawada T. Study on performance evaluation of heavy-duty anticorrosive coating for telecommunication facilities by dynamic viscoelasticity. Bosei-Kanri. 2011; 55:449–454.

[7] Kamisho T. Takeshita Y. Sakata S. Sawada T. Aging behaviour of water-based and solvent-based coatings in dry and wet environments. Bosei-Kanri. 2013; 57:451–457.

[8] Kawai H, editor. Handbook of Industrial Coating. 1st ed. Techno System: Tokyo; 2008. 256 p.

[9] Kamisho T. Takeshita Y. Sakata S. Sawada T. Water absorption of water-based anticorrosive coatings and its effect on mechanical property and adhesive performance. J. Coat. Tech. Res. 2014; 11:199–205. doi: 10.1007/s11998-013-9517-z

[10] Takeshita Y. Becker E. Sakata S. Kamisho T. Miwa T. Sawada T. Water absorption and degraded stress relaxation behaviour in water-borne anticorrosive urethane/epoxy coatings. J. Chem. Chem. Eng. 2015; 9:75–89. doi: 10.17265/1934-7375/2015.02.001

[11] Takeshita Y., Becker E., Sakata S., Miwa T., Sawada T. States of water absorbed in water-borne urethane/epoxy coatings. Polymer. 2014; 55:2505–2513. doi: 10.1016/j.polymer.2014.03.027

[12] Perera Y. D. Physical ageing of organic coatings. Prog. Org. Coat. 2003; 47:61–76. doi: 10.1016/S0300-9440(03)00037-7

[13] Sell C. G., McKenna G. B. Influence of physical ageing on the yield response of model DGEBA/poly(propylene oxide) epoxy glasses. Polymer. 1992; 33:2103–2113. doi: 10.1016/0032-3861(92)90876-X

[14] Hutchinson M. J. Physical aging of polymers. Prog. Polym. Sci. 1995; 20:703–760. doi: 10.1016/0079-6700(94)00001-I

[15] Mijovic J., Devine S. T., Ho T. Physical aging in poly(methyl methacrylate)/poly(styrene-co-acrylonitrile) blends. I. Stress relaxation. J. Appl. Polym. Sci. 1990; 39:1133–1151. doi: 10.1002/app.1990.070390509

[16] Ho T., Mijovic J., Lee C. Effect of structure on stress relaxation of polymer blends in glassy state. Polymer. 1991; 32, 619–627. doi:10.1016/00323861(91)90473V

[17] Mijovic J., Ho T., Kwei K. T. Physical aging in poly(methyl methacrylate)poly(styrene-co-acrylonitrile) blends. Part II: Enthalpy relaxation. Polym. Eng. Sci. 1989; 29:1604–1610. doi: 10.1002/pen.760292210

[18] Tavares C. A., Gulmine V. J., Lepienski M. C., Akcelrud L. The effect of accelerated aging on the surface mechanical properties of polyethylene. Polym. Degrad. Stab. 2003; 81,367–373. doi: 10.1016/S0141-3910(03)00108-3

[19] Gulmine V. J., Janissek R. P., Heise M. H., Akcelrud L. Degradation profile of polyethylene after artificial accelerated weathering. Polym. Degrad. Stab. 2003; 79:385–397. doi: 10.1016/S0141-3910(02)00338-5

[20] Cook D. W., Mehrabi M., Edward H. G. Ageing and yielding in model epoxy thermosets. Polymer. 1999; 40:1209–1218. doi: 10.1016/S0032-3861(98)00343-7

[21] Sell G. C., McKenna B. G. Influence of physical aging on the yield behavior of model DGEBA/poly(propylene oxide) epoxy glasses. Polymer. 1992; 33:2103–2113. doi: 10.1016/0032-3861(92)90876-X

[22] Kong S. E. Physical aging in epoxy matrices and composites. in Advances in Polymer Science 80, Springer-Verlag: Berlin Heidelberg;1986. 125 p. doi: 10.1007/3–540-16423-5_14

[23] Davis J. W., Pethrick A. R. Investigation of physical ageing in polymethylmethacrylate using positron annihilation, dielectric relaxation and dynamic mechanical thermal analysis. Polymer 1998; 39: 255–266. doi: 10.1016/S0032-3861(97)00392-3

[24] Robertson G. C., Wilkes L. G., Physical aging behavior of miscible blends of poly(methyl methacrylate) and poly(styrene-co-acrylonitrile). Polymer. 2001; 43,1581–1589. doi: 10.1016/S0032-3861(00)00556-5

[25] Fechine J. M. G., Rabello S. M., Souto-Maior M. R., Catalani H. L. Surface characterization of photodegraded poly(ethylene terephthalate). The effect of ultraviolet absorbers. Polymer. 2004; 45:2303–2308. doi: 10.1016/j.polymer.2004.02.003

[26] Fechine J. M. G., Rabello S. M., Souto-Maior M. R. The effect of ultraviolet stabilizers on the photodegradation of poly(ethylene terephthalate). Polym. Degrad. Stab. 2002; 75:153–159. doi: 10.1016/S0141-3910(01)00214-2

[27] Cowie M. G. J., Harris S., McEwen J. I. J. Physical ageing in poly(vinyl acetate) 1. Enthalpy relaxation. Polym. Sci. B. 1997; 35:1107–1116. doi: 10.1002/(SICI)1099-0488(199705)35:7 <1107::AID-POLB9>3.0.CO;2-S

[28] Linde van der R. Belder G. E., Perera Y. D. Effect of physical aging and thermal stress on the behavior of polyester/TGIC powder coatings. Prog. Org. Coat. 2000; 40:215–224. doi: 10.1016/S0300-9440(00)00125-9

[29] Perera Y. D., Schutyser P. Effect of physical aging on thermal stress development in powder coatings. Prog. Org. Coat. 1994; 24.299–307. doi: 10.1016/0033-0655(94)85021-6

[30] Perera Y. D., Eynde V. D. Moisture and temperature inducted stresses (hygrothermal stresses) in organic coatings. J. Coat. Technol. 1987; 59:55–63.

[31] Skaja A., Fernando D., Croll S. Mechanical property changes and degradation during accelerated weathering of polyester-urethane coatings. JCT Res.. 2006; 3:41–45. doi: 10.1007/s11998-006-0004-7

[32] Perera Y. D. Effect of thermal and hygroscopic history on physical ageing of organic coatings. Prog. Org. Coat. 2002; 44: 55–62. doi: 10.1016/S0300-9440(01)00241-7

[33] Grentzer H. T., Holsworth M. R., Provder T. The application of the dynamic mechanical analyzer to organic coatings. ACS Org. Coat. Plastics. 1981; 44: 515–519

[34] Perera Y. D., Schutyser P. Effect of physical aging on properties of organic coatings. In: Proceedings of the 22nd FATIPEC Congress vol. 1; 1994; Budapest. p. 25–38

[35] Skrovanek J. D., Schoff K. C., Thermal mechanical analysis of organic coatings. Prog. Org. Coat. 1988; 16:135–163. doi: 10.1016/0033-0655(88)80011-6

[36] Chang P. E. Viscoelastic windows of pressure-sensitive adhesives. J. Adh. 1991; 34:189–200. doi: 10.1080/00218469108026513

[37] Kaelble H. D. Peel adhesion: Influence of surface energies and adhesive rheology. J. Adh.. 1969; 1: 102–123. doi: 10.1080/00218466908078882

[38] Gent N. A., Petrich P. R. Adhesion of viscoelastic materials to rigid substrates. Proc. Roy. Soc. A. 1969; 310:433–448. doi: 10.1098/rspa.1969.0085

[39] Chan H. K., Howard J. G., Structure-property relationships in acrylic adhesives. J. Adh. 1978; 9:279–304. doi:10.1080/00218467808075121

[40] Gent N. A., Hamed R. G. Peel mechanics. J. Adh. 1975; 2:91–95. doi: 10.1080/00218467508075041

[41] Kraus G., Rollmann W. K., Gray A. R. Tack and viscoelasticity of block copolymer based adhesives. J. Adh. 1979; 10:221–236. doi: 10.1080/00218467908544626

[42] Class B. J., Chu G. S. The viscoelastic properties of rubber–resin blends. I. The effect of resin structure. J. Appl. Polym. Sci. 1985; 30:805–814. doi: 10.1002/app.1985.070300229

[43] Class B. J., Chu G. S. The viscoelastic properties of rubber–resin blends. II. The effect of resin molecular weight. J. Appl. Polym. Sci. 1985; 30:815–824. doi: 1002/app. 1985.070300230

[44] Class B. J., Chu G. S. The viscoelastic properties of rubber–resin blends. III. The effect of resin concentration. J. Appl. Polym. Sci. 1985; 30:825–842. doi: 10.1002/app. 1985.070300231

[45] Chu G. S. in Chapter 8, Viscoelastic properties of pressure-sensitive adhesives, D. Satas, editor. Handbook of Pressure Sensitive Adhesive Technology. Van Nostrand Reinhold: New York (1989).

[46] Takemura A., Kuriyama H., Moriguchi T., Tomita B., Mizumachi H., Dynamic mechanical properties and adhesive strengths of polyacrylates I. Mokuzai Gakkaishi. 1986; 32:813–819 (in Japanese)

[47] Ochi K., Iwakoshi M., Niiho M. Properties of cured epoxide resins (Part 2). J. Adh. Soc. Jpn. 1974; 10:266–272 (in Japanese).

[48] Motohashi K., Toota B., Mizumachi H., Sakaguchi H. Temperature dependency of bond strength of polyvinyl acetate emulsion adhesives for wood. Wood Fiber Sci. 1984; 16:72–85.

[49] Mizumachi H., Hatano Y., Yamagishi Y., Keon L. Influence of the mechanical properties of plasticized polymers on wood adhesion. Holzforschung. 1983; 37:153–156. doi: 10.1515/hfsg.1983.37.3.153

[50] Mizumachi H., Tsukiji M. Interaction between wood and polymers. Pt. VI. Dynamic mechanical properties of polymers filled with wood components. Hozforschung. 1980; 34:122–124. doi: 10.1515/hfsg.1980.34.4.122

[51] Kobayashi M., Hatano Y., Tomita B. Viscoelastic properties of liquefied wood/epoxy resin and its bond strength. Holzforschung. 2001; 55:667–671. doi: 10.1515/HF.2001.108

[52] Mizumachi H., Fujino M. Interaction between wood and polymers. Holzforschung. 1972; 26:164–169. doi: 10.1515/hfsg.1972.26.5.164

[53] Takemura A., Tomita B., Mizumachi H., Dynamic mechanical properties and adhesive strengths of epoxy resins modified with liquid rubber. I. Modification with ATBN. J. Appl. Polym. Sci. 1985; 30:4031–4043. doi: 10.1002/app.1985.070301007

[54] Takemura A., Shiozawa K., Tomita B., Mizumachi H. Dynamic mechanical properties and adhesive strengths of epoxy resins modified with liquid rubber. II. Modification with CTBN. J. Appl. Polym. Sci. 1986; 31:1351–1362. doi: 10.1002/app.1986.070310519

[55] Davies R. O., Jones G. O. The irreversible approach to equilibrium in glasses. Proc. Roy. Soc. A.1953; 217:26–42. doi: 10.1098/rspa.1953.0044

[56] Davies R. O., Jones G. O. Thermodynamic and kinetic properties of glasses. Adv. Phys. 1953; 2:370–410. doi: 10.1080/00018735300101252

[57] The Society of Rheology, Japan. What's rheology? Available from: http://www.srj.or.jp/index-j.html [Accessed: 2016-05-02]

[58] Crank J. 9.4. Sorption- and desorption-time curves. 10.6.7 Use of initial rates of sorption and desorption. In The Mathematics of Diffusion. 2nd ed. Oxford University Press; Oxford; 1975. p. 179–189 and 244–246. ISBN-10: 0198534116

[59] Ferry D. J. In Viscoelastic Properties of Polymers. 3rd ed. John Wiley & Sons: New York; 1980. ISBN: 978–0-471–04894-7

[60] Williams G., Watts C. D. Non-symmetrical dielectric relaxation behaviour arising from a simple empirical decay function. Trans. Faraday. Soc. 1970; 60:80–85. doi: 10.1039/TF9706600080

[61] Hetman P., Szabat B., Weron K., Wodziński D. 2003. On the rajagopal relaxation-time distribution and its relationship to the Kohlrausch–Williams–Watts relaxation function. J. Non-Cryst. Solids. 2003; 330:66–74. doi: 10.1016/j.jnoncrysol.2003.08.060

[62] Johnston D. Stretched exponential relaxation arising from a continuous sum of exponential decays. Phys. Rev. B. 2008; 74:184430–1-184430–7. doi: http://dx.doi.org/10.1103/PhysRevB.74.184430

[63] Lindsey, C. P., Patterson G. D. Detailed comparison of the Williams–Watts and Cole–Davidson functions. J. Chem. Phys. 1980; 73:3348–3357. doi: http://dx.doi.org/10.1063/1.440530

[64] Weron K. Relaxation in glassy materials from lévy stable distributions. Acta Physica Polonica A. 1986; 70:529–539.

[65] Barton J. M. Effect of absorbed water on the thermal relaxation of biaxially stretched crosslinked poly(methyl methacrylate. Polymer. 1979; 20:1018–1024. doi: 10.1016/0032-3861(79)90202-7

[66] Baschek G. Hartwig G. Zahradnik F. Effect of water absorption in polymers at low and high temperatures. Polymer. 1999; 40:3433–3441. doi: 10.1016/S0032-3861(98)00560-6

[67] Yoon S. C., Ratner B. D. Surface and bulk structure of segmented poly(ether urethanes) with perfluoro chain extenders. 2. FTIR, DSC, and X-ray photoelectron spectroscopic studies. Macromolecules.1988; 21:2392–2400. doi: 10.1021/ma00186a016

[68] Funke W. Zorll U. Murthy B. G. Interfacial effects in solid paint films related to some film properties. J Paint Technol. 1969; 41: 210–221.

[69] Sperling L. H. Introduction to Physical Polymer Science. 4th ed. Wiley; Hoboken, New Jersey; 2005. ISBN: 978-0-471-70606-9

[70] Bahar I., Erman B., Fytas G., Steffen W. Intramolecular contributions to stretched-exponential relaxation behavior in polymers. Macromolecules.1994; 27:5200–5205. doi: 10.1021/ma00096a051

[71] Ping Z. H., Nguyen Q. T., Chen S. M., Zhou J. Q., Ding Y. D. States of water in different hydrophilic polymers — DSC and FTIR studies. Polymer. 2001; 42:8461–8467. doi: 10.1016/S0032-3861(01)00358-5

[72] Rosa F., Bordado J., Casquilho M. Kinetics of water absorbency in AA/AMPS copolymers: applications of a diffusion–relaxation model. Polymer. 2002; 43:63–70. doi: 10.1016/S0032-3861(01)00596-1

[73] Nogueira P., Ramarez C., Torres A., Abad M. J., Cano J., Lopez J. Effect of water sorption on the structure and mechanical properties of an epoxy resin system. J. Appl. Polym. Sci. 2001; 80:71–80. doi: 10.1002/1097-4628(20010404)80:1<71::AID-APP1077>3.0.CO;2-H

[74] Higuchi A., Iijima T. D.S.C. investigation of the states of water in poly(vinyl alcohol) membranes. Polymer. 1985; 26: 1207–1211. doi: 10.1016/0032-3861(85)90254-X

[75] Higuchi A., Iijima T. D.S.C. investigation of the states of water in poly(vinyl alcohol-co-itaconic acid) membranes. Polymer. 1985; 26: 1833–1837. doi: 10.1016/0032-3861(85)90011-4

[76] Liu W. G., Yao K. D. What causes the unfrozen water in polymers: hydrogen bonds between water and polymer chains? Polymer. 2001; 42:3943–3947. doi:10.1016/S0032-3861(00)00726-6

[77] Musto P., Ragosta G., Mascia L. Vibrational spectroscopy evidence for the dual nature of water sorbed into epoxy resins. Chem. Mater. 2000; 12;1331–1341. doi: 10.1021/cm9906809

[78] Mijovic J., Zhang H. Local dynamics and molecular origin of polymer network-water interactions as studied by broadband dielectric relaxation spectroscopy, FTIR, and molecular simulations. Macromolecules. 2003; 36:1279-1288. doi: 10.1021/ma021568q

[79] Cotugno S., Mensitieri G., Musto P., Sanguigno L. Molecular interactions in and transport properties of densely crosslinked networks: a time-resolved FT-IR spectroscopy investigation of the epoxy/H_2O system. Macromolecules. 2005; 38:801–811. doi: 10.1021/ma040008j

[80] Harazaki Y. Fundamental Science of Coatings. 1st ed. Maki Press: Tokyo; 1977. 32 p.

IntechOpen